solids

MDPI

Review

Stability and Degradation of 2D Materials Based Heterostructure Electrocatalysts in Electrochemical Energy Conversion

Om Prakash Gujela [1,2], Mario Hofmann [3] and Ding-Rui Chen [4,*]

[1] Graduate Institute of Applied Physics, National Taiwan University, Taipei 106319, Taiwan; opgujela@gmail.com
[2] Department of Electrical and Electronics Engineering, Bakhtiyarpur College of Engineering, Bihar Engineering University, Patna 800001, India
[3] Department of Physics, National Taiwan University, Taipei 106319, Taiwan; mario@phys.ntu.edu.tw
[4] Department of Electronic Engineering, Chung Yuan Christian University, Taoyuan 320, Taiwan
* Correspondence: drchen30@cycu.edu.tw

Abstract

Two-dimensional (2D) heterostructures offer tunable electronic structures and synergistic interactions that enhance electrocatalytic activity beyond the limits of single-component materials. However, the same atomically thin interfaces that enable high performance also introduce inherent mechanical, chemical, and electronic vulnerabilities, giving rise to complex and coupled degradation pathways. In this review, we provide a systematic overview of degradation in 2D heterojunction electrocatalysts during electrochemical operation, covering failure mechanisms, operando characterization, and stabilization strategies. Degradation is governed by interfacial strain accumulation, bubble-induced stress and delamination, galvanic corrosion, and selective leaching, while stability can be improved through interfacial coupling, structural confinement, and controlled reconstruction. These insights provide practical design guidelines for developing robust 2D heterostructures for electrochemical energy conversion.

Keywords: 2D heterostructures; electrocatalysis; interfacial stability; degradation mechanisms; operando characterization

1. Introduction

Catalysis is crucial for clean and sustainable technologies by enabling electrochemical energy conversion that uses renewable electricity to produce clean energy [1,2]. Two-dimensional (2D) materials are considered cost-effective and highly efficient candidates for electrochemical energy conversion because of their high density of exposed atoms and their uniquely tunable structures [3,4]. However, pure 2D mono-layers still face fundamental limitations, including high baseline resistance and chemically inert surfaces [5].

To address these limitations, heterostructure engineering has become an influential strategy [6–8]. The combination of two or more catalytic components was shown to surpass the performance of single-component catalysts [9–11] through electronic interactions [12], beneficial crystallography [13], and synergistic cooperation between adjacent catalysts [14,15].

Although the formation of heterostructures significantly enhances catalytic activity [16], they simultaneously introduce critical vulnerabilities in electrochemical stability [16–19]. Indeed, significant research is aiming at balancing catalytic enhancement with degradation stability [20,21]. To achieve this goal, a firm grasp of the multistep, multi-scale, and reaction-dependent nature of degradation in 2D heterostructures is required [22,23].

Check for updates

Academic Editor: Stefano Agnoli

Received: 4 March 2026
Revised: 30 March 2026
Accepted: 30 March 2026
Published: 2 April 2026

Copyright: © 2026 by the authors. Licensee MDPI, Basel, Switzerland. This article is an open access article distributed under the terms and conditions of the Creative Commons Attribution (CC BY) license.

This review aims to provide a systematic overview of degradation in 2D heterostructure electrocatalysts. We first classify the dominant mechanical, electrochemical, and thermodynamic failure modes, highlighting reaction-specific pathways in the hydrogen evolution reaction (HER), oxygen evolution reaction (OER), carbon dioxide reduction reaction (CO_2RR), and nitrogen reduction reaction (NRR). We then discuss the emerging landscape of advanced characterization and metrology that distinguish intrinsic degradation from measurement artifacts. Finally, we highlight stabilization strategies that could lead to durable 2D heterostructure electrocatalysts for practical electrochemical energy conversion.

2. Degradation Mechanisms in 2D Heterostructures

The degradation in 2D heterostructures is a coupled cascade of mechanical, electrochemical, and reaction-specific failures [24,25]. This section categorizes these fundamental mechanisms and highlights the specific electrochemical processes where each failure mode remains dominant.

2.1. Mechanical Failure: Lattice Mismatch and Hydrodynamic Fatigue

Mechanical degradation in 2D heterostructures is fundamentally distinct from bulk composite failure; it is governed not by the accumulation of misfit dislocations, but by the incompatibility of elastic moduli and the weak nature of the van der Waals (vdW) interface. The chemically inert basal planes of 2D materials lead to weak interfacial adhesion governed by vdW forces [26], whose binding energies are typically one to two orders of magnitude lower than those of covalent or ionic bonds [27,28]. In heterostructures composed of dissimilar crystal structures (e.g., chalcogenides on oxides), a static lattice mismatch (f) generates significant elastic strain energy at the junction [28,29]. Unlike bulk composites where stress is released via grain boundary dislocations, atomically thin 2D interfaces accommodate this mismatch through the formation of continuous elastic strain fields [28]. As illustrated in Figure 1, these intrinsic strain effects can emerge from various structural origins, including morphology, defects, substrate interactions, and lattice mismatch, which collectively concentrate elastic strain energy at the heterointerface, thereby reducing the structural integrity.

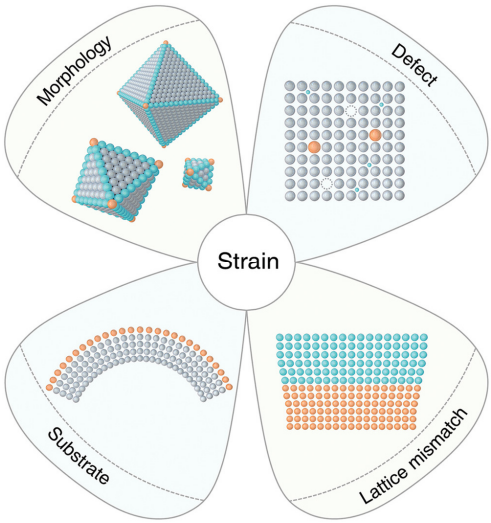


Figure 1. Atomic-scale representation of lattice mismatch in a vdW heterostructure. The difference in lattice constants between the substrate (cyan) and the over-layer (orange) produces a continuous strain field across the interface despite the absence of misfit dislocations. This mismatch-driven strain concentrates elastic energy at the heterointerface and serves as the primary origin for the structural instability mechanisms described in the main text. Adapted with permission from [29].

Following the attenuation of the interface by intrinsic strain, the system becomes highly susceptible to extrinsic hydrodynamic forces, specifically bubble-induced shear stress. In high-current gas-evolving processes (HER/OER), the stability of the catalyst is controlled by a critical force equilibrium formulated in the framework of the Wenzel wetting model [30]. For 2D materials with flat basal planes, the electrolyte infiltrates surface irregularities, forming a continuous three-phase contact line (TPCL) that anchors gaseous bubbles to the surface [31]. This anchoring increases the capillary adhesion force (F_{ad}), allowing bubbles to reach millimeter dimensions before detachment [30,32]. These immobilized bubbles produce "dead zones" that inhibit ion transport; more critically, they impose considerable tensile stress perpendicular to the interface [32].

If the bubble adhesion force (F_{ad}) exceeds the interfacial binding force ($F_{binding}$), the catalyst layer is mechanically stripped along with the detaching bubble [30,33]. This bubble-induced interfacial delamination is particularly harmful under industrial current densities (>500 mA cm^{-2}), where the combination of rapid bubble nucleation and coalescence creates large shear forces that easily overcome these weak interactions, leading to material washout regardless of the intrinsic chemical stability of the catalyst [20,33]. Moreover, the incorporation of electrolyte ions into the interfaces of loosely stacked 2D materials may initiate structural expansion and promote the erosion of the underlying substrate [20,34].

2.2. Electrochemical and Thermodynamic Instability

Electronic coupling and electrochemical corrosion processes also play a major role in the thermodynamic stability [35,36]. Strong electronic coupling at the heterointerface promotes charge redistribution and generation of built-in electric fields, which boost the electron transfer kinetics [37]. Simultaneously, localized charge accumulation can lead to the destabilization of the electron-donating component, making it prone to self-oxidation or the selective leaching [20,38]. For instance, in metal/semiconductor junctions, the formation of a Schottky barrier hinders electron transport and the increased interfacial resistance promotes localized electrochemical corrosion if not mitigated through proper Ohmic-contact engineering [39].

These processes can be understood by the thermodynamic incompatibility of the coupled phases under electrochemical bias. Within heterojunctions, the chemical stability is no longer determined by the intrinsic Pourbaix diagrams of individual materials, but instead by the equilibrated Fermi level and the interfacial electric field. A major degradation pathway is interfacial selective leaching, driven by the work-function difference ($\Delta\Phi$) between the 2D catalyst and its conductive support [38,40]. Upon contact, spontaneous electron transfer equilibrates the Fermi levels, often rendering the active phase electron-deficient (anodic). This reduction in electron density weakens metal–ligand covalent bonds (e.g., Mo–S, Co–P) and lowers the dissolution potential, enabling oxidative leaching ($M \rightarrow M^{n+}$) at potentials where the isolated catalyst would remain stable—thus turning a synergistic electronic effect into a pathway for accelerated corrosion [41,42].

Beyond galvanic effects, multi-component heterostructures (e.g., metal-doped dichalcogenides or LDH/MXene hybrids) frequently suffer from selective leaching. The constituent elements in these hybrids often exhibit disparate electrochemical stability windows. Under the high anodic potentials required for the OER (>1.5 V vs. the reversible hydrogen electrode (RHE)), thermodynamically unstable elements such as Zn, Al or V preferentially leach into the electrolyte, a process frequently termed "sacrificial activation" [43,44]. Although this process is initially shown to augment catalytic activity by creating active vacancies and increasing the electrochemically active surface area (ECSA), excessive leaching inevitably leads to the structural collapse of the host lattice framework [45]. Such a drift in stoichiometry alters the local coordination environment of the remaining active sites, resulting in a

gradual loss of intrinsic activity and eventually the electrical isolation of catalyst clusters from the current collector [40,43].

A further challenge is interface-dependent phase metastability. Many high-performance electrocatalysts utilize metastable phases, such as metallic 1T-MoS_2 or 1T-WSe_2, which exhibit superior conductivity compared to their 2H analogs [38,46]. The kinetic stabilization of these phases is often possible using electron-donating supports (e.g., N-doped graphene) that raise the activation energy barrier for the 1T to 2H transition [38,47]. However, this creates a relational dependency: if mechanical decoupling or delamination occurs—as detailed in the mechanical degradation section—the metastable phase loses its extrinsic stabilization and relaxes to its inert ground state, causing a sudden loss in catalytic activity [20,38].

Finally, electrochemical corrosion of the support often limits heterostructure lifetime, especially in carbon-based systems (graphene, CNTs). Carbon supports are thermodynamically unstable above 0.207 V vs. RHE and are oxidized to CO_2 [48]. Active metals such as Pt, Co and Ni catalyze this oxidation, lowering the activation energy and accelerating carbon loss. As the substrate is consumed, 2D nanosheets detach from the electrode—a failure mode known as interfacial detachment—underscoring that the chemical inertness of the support must be engineered with the same rigor as the catalyst itself.

2.3. Other Mechanisms

Pore clogging from carbonate precipitation is a degradation pathway unique to alkaline or neutral CO_2RR systems [49,50]. During high-current-density operation, local pH near the cathode rises sharply due to proton consumption and hydroxide generation [51]. The resulting alkaline microenvironment reacts with the incoming CO_2 feed to form carbonate and bicarbonate species, which crystallize within the confined nano-scale gaps of 2D heterostructures [51,52]. This precursor addition mechanism—opposite to the dissolution-driven degradation typical of HER/OER—leads to "salt flooding" of the gas diffusion electrode (GDE). The accumulated precipitates block mesoporous channels, impose severe diffusion barriers, starve active sites of CO_2, and permanently divert the reaction toward water reduction [51,53].

In addition, wetting transitions ("flooding") compromise the stability of GDEs used in industrial CO_2RR. Maintaining a stable solid–liquid–gas triple-phase boundary typically requires hydrophobic surfaces [54]. However, under sustained cathodic polarization, electrowetting and the accumulation of liquid products (e.g., ethanol, formate) decrease interfacial tension and allow electrolyte intrusion into hydrophobic pores [55,56] This transition collapses the fast gas-phase transport regime into a slow liquid-phase diffusion regime. Without periodic regeneration, the flooding becomes structurally irreversible and is one of the primary lifetime-limiting factors in flow-cell electrolyzers [54,57].

A unified overview of degradation pathways for important electrocatalytic processes are summarized in Table 1.

Table 1. Summary of reaction-specific failure modes in 2D heterostructure electrocatalysts.

Reaction	Dominant Environmental Stressor	Primary Interfacial Failure Mode	Key Mechanism	Reference
HER	H^+ Intercalation/Gas Bubbles	Physical Delamination	Lattice breathing (volume expansion) & bubble shear stress ($F_{shear} > F_{adhesion}$)	[32,58]
OER	High Anodic Potential (>1.5 V)	Crystalline Defect Formation	Lattice Oxygen Oxidation Mechanism (LOM) & segregation of soluble species (e.g., V, Zn leaching)	[43,59]
CO_2RR	Local pH change/Intermediates	Selectivity Decay	Carbonate precipitation blocking pores & poisoning of active sites by *CO/*CHO	[51,52]
NRR	Competitive HER	Surface Reconstruction	Amorphization of crystalline interfaces & active site poisoning by H*	[60,61]
Dynamic Reactions	Start-Stop Cycling	Interfacial Fatigue	Repeated expansion/contraction cycles severing weak van der Waals contacts	[28,55]

3. Characterization and Metrology

Evaluating the stability of 2D heterostructures requires metrology far more sophisticated than the durability tests commonly applied to bulk or three-dimensional catalysts. Standard protocols such as chronopotentiometry and ex situ characterization often fail to detect the buried, nano-scale, and reaction-coupled degradation pathways that dominate atomically thin interfaces. Because mechanical delamination, selective dissolution, electronic decoupling, and phase relaxation can all occur without perturbing the geometric current or the apparent ECSA, traditional measurements frequently yield misleading "false-positive" indicators of stability. Accurate lifetime assessment therefore demands an integrated framework that couples quantitative electrochemical metrics with operando structural and electronic probes capable of resolving dynamic changes at the heterojunction interface. This section summarizes the metrological challenges unique to 2D heterostructures and outlines state-of-the-art techniques from S-number analysis and high-frequency impedance to operando transmission electron microscopy (TEM), electrochemical tip-enhanced Raman spectroscopy (EC-TERS), and X-ray absorption spectroscopy (XAS), which reliably identify intrinsic degradation mechanisms.

3.1. Electrochemical Characterization of Degradation

Standard durability protocols, while useful for initial screening, often fail to capture the subtle interfacial degradation modes unique to 2D heterostructures. A rigorous assessment of stability requires moving beyond simple current retention to advanced metrology capable of distinguishing between intrinsic catalytic lifetime and measurement artifacts.

Conventional chronopotentiometry (CP) conducted at low current densities (<10 mA cm^{-2}) is frequently cited as proof of durability; however, this metric often yields unreliable stability results. Since the exfoliation of degraded layers exposes fresh active sites, a constant current density can be achieved despite mass loss [56,62]. Chen et al. observed that during the degradation of NiFe-LDH, the selective leaching of sacrificial elements (e.g., Al or Zn) or the delamination of nanosheets roughened the surface, leading to a spike in capacitance even as the intrinsic catalytic activity plummeted [63]. This phenomenon, where electrochemically active surface area (ECSA) or double-layer capacitance (C_{dl}) increases despite actual catalyst degradation, is herein referred to as the "ECSA paradox." It arises because surface roughening, delamination, or selective leaching can expose fresh active sites or increase apparent surface area, thereby masking the intrinsic loss of catalytic activity.

To address this issue, performance can be normalized by the Site-Specific Turnover Frequency (TOF), which quantifies the activity per surviving active site rather than the geometric area, revealing the true kinetic degradation hidden by surface roughening [63,64]. Another approach is the "stability number" (S-number), introduced by Escalera-López et al. [65], defined as the ratio of the amount of evolved gas (hydrogen or oxygen) to the amount of dissolved metal ions quantified via flow-cell Inductively Coupled Plasma Mass Spectrometry (ICP-MS). As illustrated in Figure 2a,b, the S-number reveals element- and structure-dependent stability trends in MoSx-based systems, with Mo exhibiting higher stability than S and crystalline phases outperforming amorphous counterparts under electrochemical operation. Unlike CP, which only tracks electron flow, the S-number provides a metric of thermodynamic corrosion resistance, effectively decoupling intrinsic stability from surface-area roughening [62,65].

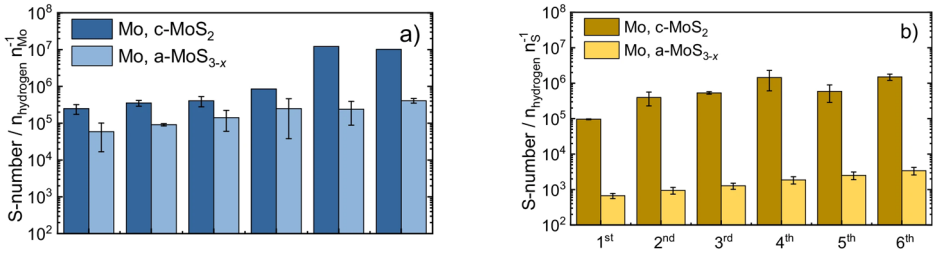


Figure 2. Graphical representation of total integrated dissolution of (**a**) Mo (blue) and (**b**) S (yellow) as a function of the LPL. Quantitative assessment of intrinsic durability using the stability number (S-number). The S-number is defined as the ratio between the amount of evolved product gas (e.g., H_2) and the number of dissolved catalyst atoms (e.g., Mo or S) measured downstream by ICP-MS. A higher S-number reflects greater catalytic turnover per atom lost, providing a durability metric that is independent of surface-area changes or peeling-induced activation. Reproduced from [65].

At high industrial current densities (>500 mA cm^{-2}), the accumulation of gas bubbles at the aerophilic heterointerface creates a stochastic "bubble overpotential" (η_{bub}) that distorts stability measurements. Standard Electrochemical Impedance Spectroscopy (EIS) often conflates this hydrodynamic noise with the intrinsic charge transfer resistance (R_{ct}). Iwata et al. demonstrated that standard iR-correction is invalid in this regime because bubble resistance is frequency-dependent [32]. Accurate stability assessment requires high-frequency impedance analysis to mathematically subtract the dynamic bubble coverage effects. This isolation is critical to distinguish between actual catalyst degradation (an increase in intrinsic R_{ct}) and simple bubble blocking effects [32,39].

3.2. Operando Visualization of Dynamic Degradation

Mechanical stress and phase instability cause 2D heterostructures to degrade in ways that are often invisible to ex situ measurements due to rapid relaxation once bias is removed. Real-time operando tools are therefore essential for resolving buried interfacial changes that govern long-term stability.

Ex situ characterization is prone to significant artifacts when applied to 2D materials. For example, "capillary re-stacking" during the drying of TEM samples can re-adhere delaminated layers, effectively hiding the physical gaps that existed during operation [28]. To visualize the true interfacial state, cross-sectional high-angle annular dark-field scanning transmission electron microscopy (HAADF-STEM) or liquid-cell operando TEM is required to image the van der Waals gap and solid–liquid interface in situ [9,66]. Liquid-cell TEM (LC-TEM) captures electrolyte–catalyst interactions with atomic resolution and directly reveals electrowetting-induced restructuring and hydrophilicity changes during cycling. However, LC-TEM suffers from beam-induced artifacts (eaq-, OH•, artificial bubbling, metal redeposition), requiring stringent control to avoid misinterpreting radiolysis effects as genuine degradation [28,66].

While structural visualization techniques capture the physical evolution of 2D heterostructures, operando XAS provides the complementary electronic perspective that is otherwise lost once the bias is removed. As illustrated in Figure 3a, a Ru K-edge X-ray absorption near-edge structure (XANES) recorded under working conditions reveals measurable shifts in the absorption edge relative to OCV, indicating a dynamic modification of the electronic environment at the active site. Corresponding Fourier-transformed (FT) EXAFS analyses (Figure 3b) further show changes in the local coordination structure, consistent with subtle bond rearrangements that occur during electrochemical operation. Quantitative analysis of the Ru oxidation state and radial distance (Figure 3c) further tracks these transient electronic fluctuations and supports the reversible nature of the active center under bias.

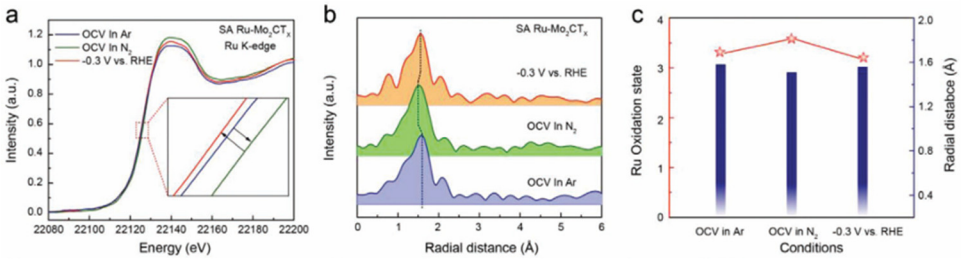


Figure 3. Operando X-ray absorption spectroscopy (XAS) of Ru active sites under varying bias. (**a**) XANES, (**b**) FT-EXAFS, and (**c**) extracted oxidation state and radial distance, revealing dynamic electronic and structural evolution during operation. Reproduced from [60].

These spectral features collectively point toward a bias-responsive redistribution of electron density at the heterointerface. This electronic redistribution has direct implications for interfacial stability. Specifically, the relatively stable XANES absorption edge and the preservation of the first coordination shell in extended X-ray absorption fine structure (EXAFS) suggest that strong electronic coupling between the active phase and the support can help stabilize the local electronic environment. This electronic coupling effect may modulate interfacial bond strength and suppress the over-oxidation of metal centers, thereby enhancing the resistance of the heterostructure to delamination or phase transformation under operating conditions.

Total Internal Reflection (TIR) imaging has proven to be an efficient technique of visualizing the buried interface between the catalyst and substrate [39]. It allows direct observation of the moment when the capillary force of a growing bubble (F_{bubble}) exceeds the interfacial adhesion (F_{ad}), capturing stick–slip dynamics and nano-scale lift-off events long before macroscopic delamination appears, enabling quantitative correlations between hydrophobicity, adhesion energy, and mechanical robustness [39,67].

At the nano-scale, EC-TERS overcomes the spatial averaging of bulk spectroscopy and provides <10 nm resolution under bias. It has been used on MoS_2 to map 2H $\rightarrow$ 1T transitions and local strain (ε_{xx}) evolution prior to crack formation, revealing that active sites are not static but dynamically deforming regions that precede failure [68].

Electronic structures must also be evaluated operando: ex situ XPS underestimates metastable states (e.g., polarized 1T-MoS_2) because they relax immediately once bias is removed. Tracking metal–support coordination under real bias therefore requires operando XAS to confirm that electron-donating pathways, such as Co–N or Ru–C bonds, remain intact [60,69].

Chemical stability is often lost through selective leaching of unstable elements—something ex situ analysis rarely resolves because dissolution occurs only in narrow potential windows or during transient cycling [65]. Scanning Flow-Cells coupled with Inductively Coupled Plasma Mass Spectrometry (SFC-ICP-MS) provide real-time ppb-level dissolution rates (e.g., Mo vs. S) [65,70]. These measurements distinguish beneficial sacrificial activation from destructive stoichiometric depletion that eventually collapses frameworks in metal-doped TMDs or NiFe-LDH [43,71].

Mechanistic visualization also requires improvement. Bubble-induced stress and catalyst peeling remain largely qualitative descriptions. Integrating high-speed in situ microscopy with electrochemical noise or current analysis is essential to quantify the actual adhesion forces responsible for delamination under operating conditions [32,39]. These experimental gaps parallel limitations in theory. Conventional density functional theory (DFT) treats interfaces as static and crystalline, despite experimental evidence of in situ amorphization, defect diffusion, and time-dependent Fermi-level shifts under bias [21,29,71]. The stability is poorly predicted by the use of purely computational models which assume that the constant changes in the Fermi level, solvation shells and strain

fields that evolve continuously throughout the reaction are ignored. Future modeling must incorporate GC-DFT and AIMD with explicit solvation to capture dynamic reconstruction and move beyond idealized binding-energy descriptors toward predictive degradation-pathway simulations [23,29].

This multimodal framework is increasingly necessary for distinguishing intrinsic material instability from artifacts arising from electrode architecture or measurement conditions, thereby offering a path toward rational design of heterostructures with truly industrial lifetimes [39,65,66].

4. Stabilization Strategies

4.1. Physical and Mechanical Reinforcement: Anchoring, Epitaxy, and Encapsulation

Interfacial peeling driven by bubble capillary forces requires replacing weak van der Waals contact with stronger chemical anchoring. Because 2D basal planes lack dangling bonds and exhibit low adhesion energies, defect-engineered supports have been widely adopted [20,72]. Introducing –COOH/–OH groups or N dopants into graphene or CNTs generates nucleation sites that form C–S–Mo or C–O–Mo bonds with MoS_2, creating "atomic rivets" with dissociation energies >100 kJ mol^{-1}. These covalent linkages raise the interfacial binding force above bubble detachment forces, suppressing delamination even at industrial current densities (~500 mA cm^{-2}) [73,74].

Mechanical degradation arising from elastic-modulus mismatch between rigid oxides and compliant chalcogenides can be mitigated through Domain-Matching Epitaxy (DME). Instead of enforcing strict lattice matching, DME pairs $\boldsymbol{m}$ unit cells of one layer with $\boldsymbol{n}$ of the other, periodically releasing residual strain and preventing crack-initiating stress accumulation during lattice breathing. Lateral (in-plane) heterostructures further eliminate the vertical vdW gap and reduce out-of-plane strain gradients, improving fatigue tolerance under dynamic operation [29,72].

To stabilize catalytically active but chemically fragile materials in acidic or alkaline media, graphene encapsulation provides a thin, corrosion-resistant barrier while maintaining electronic continuity. Unstable metal phosphides and non-noble alloys (e.g., CoNi) can be wrapped by 1–3 graphene layers that prevent direct electrolyte contact. The electron-penetration effect enables charge transfer through the graphene shell, preserving activity while strongly suppressing oxidative dissolution and extending operational lifetimes to hundreds or thousands of hours [75,76].

Maintaining gas-transport pathways is equally important. Flat 2D layers favor a Wenzel wetting state, trapping bubbles and inducing local tensile strain associated with "wicking-mode" failure. Superaerophobic 3D architectures—constructed by vertically integrating 2D sheets onto conductive nanoarrays (e.g., NiCoP arrays, carbon cloth)—create discontinuous triple-phase contact lines that drastically reduce bubble adhesive forces. Rapid bubble release minimizes mechanical loading, prevents electrolyte blockage, and mitigates dead-zone formation that accelerates material washout [32,77].

Finally, preventing substrate-induced failure requires mechanically robust supports. Carbon supports oxidize above ~1.5 V vs. RHE and often fail through substrate corrosion-driven detachment. Nanoconfinement strategies using mesoporous oxides, nitrides, or nanoporous gold (NPG) create rigid–flexible coupled scaffolds that accommodate intercalation-induced stress. Confining MoS_2 within such frameworks limits volume expansion during start–stop cycling and preserves electrical contact—a structural remedy for the intrinsic mechanical fragility of 2D materials [57,78].

4.2. Electronic and Thermodynamic Immunization

Thermodynamic stability in 2D heterostructures ultimately depends on controlling electron flow across the interface. Consequently, a work function mismatch (Φ) produces spontaneous galvanic corrosion. For example, a 2D layer becomes anodic upon contacting high-Φ supports (e.g., Au, Pt), resulting in degradation [38,41]. A solution is the coupling of the catalyst with low-work-function, electron-donating substrates—including CeO_2 or N-doped graphene—in 1T-MoS_2 systems which pins the Fermi level and continuously injects electrons into metal–chalcogen orbitals, preserving metal–ligand covalency and preventing oxidative dissolution at high potentials [38,40]. As illustrated in Figure 4a,b, modulation of the d-band center and antibonding states governs the adsorption strength of oxygenated species. This provides a basis for understanding how interfacial electronic coupling in heterostructures can influence catalytic stability.

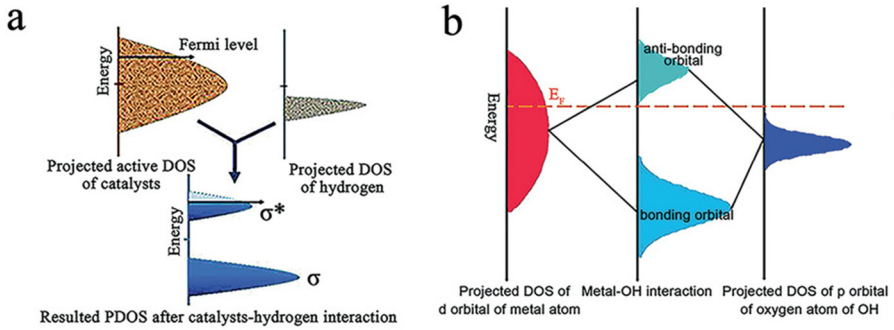


Figure 4. Schematic illustration of electronic structure modulation and its influence on adsorption strength. (**a**) Orbital hybridization between the catalyst d-band and hydrogen s-band, forming bonding (σ) and antibonding (σ*) states. (**b**) Interaction between the metal d-orbital and the p-orbital of oxygen atoms in OH intermediates. The occupancy of antibonding states influences the binding strength and is closely associated with stability against oxidative dissolution. Reproduced from [5].

Beyond electronic buffering, metastable metallic phases (e.g., 1T-MoS_2, 1T′-WSe_2) require interfacial coordination to resist relaxation into their 2H ground states [46]. Planar macrocycles such as FePc act as "coordination rivets," locking surface atoms into octahedral geometries and raising the kinetic barrier for phase reversion. Additional steric confinement—through interlayer intercalation of Li^+/Na^+ or small molecules—further suppresses layer sliding and maintains conductivity over extended cycling [28,47].

Electronic stabilization also depends on tuning the d-band center (ε_d). Interfacial strain or strong coupling in heterostructures (e.g., Ir/MoO_2, Pd/Au) downshifts ε_d, weakening the adsorption of oxygenated intermediates (OH*, O*) that typically trigger over-oxidation. Optimizing ε_d allows a balanced regime where active sites retain sufficient binding strength for catalysis yet remain resistant to forming high-valence inactive species during OER [29,72].

For alkaline OER and other highly oxidative environments, sacrificial-leaching engineering provides a controlled route toward a self-passivating, active surface. Introducing thermodynamically unstable elements (e.g., Zn, Al, V in LDH or doped TMDs) promotes preferential leaching under anodic bias, forming a cation-deficient, amorphous reconstruction layer enriched in high-valence active species (such as NiOOH) [43]. Unlike uncontrolled dissolution that collapses the lattice, this reconstruction is self-limiting and preserves a conductive crystalline core [45,79].

Finally, incorporating redox-active ions (e.g., Co^{2+}, Fe^{3+}) into the electrolyte enables dynamic self-healing: dissolved species re-crystallize onto the electrode when the potential sweeps or equilibrium fluctuates, maintaining constant stoichiometry and site density. This

regeneration mechanism represents a path toward sustained activity in non-noble-metal heterostructures under industrial current densities [39,53].

A summary of representative stabilization strategies and their demonstrated durability across heterogeneous systems is provided in Table 2.

Table 2. Representative stabilization strategies for 2D heterostructure electrocatalysts.

Heterostructure System	Stabilization Strategy	Stability Test Condition	Lifetime/Performance	Refences
$Ti_3C_2T_x$ @5Pt (MXene/Pt)	Covalent anchoring (Ti–Pt bonds)	0.5 M H_2SO_4, HER, −10 mA cm^{-2}	800 h (No decay)	[80]
NiFe LDH@NiCoP/NF	3D hierarchical gas release (Superaerophobicity)	1.0 M KOH, OER, 100 mA cm^{-2}	100 h (Stable potential)	[77]
Co@NC (Co/Graphene)	"Chain mail" encapsulation (Electron Penetration)	0.5 M H_2SO_4, HER	1000 h (Acid stable)	[75]
NiFe LDH-NS@DG	Defect anchoring (trapped in graphene defects)	1.0 M KOH, OER	Negligible decay after 1000 cycles	[73]
Mo_2CN@C/PbNC	Interfacial bonding (Mo–N/C bonds)	0.1 M Na_2SO_4, NRR	High NH_3 yield retention	[81]
2D MoS_2/50CNT	Conductive scaffolding (preventing restacking)	0.5 M H_2SO_4, HER	Optimal charge transfer (R_{ct}/min)	[74]

5. Conclusions

The stability of 2D heterostructure electrocatalysts is determined by a combination of mechanical, chemical, and electronic processes that originate at the interface and evolve during operation. The research discussed in this review indicates that degradation commonly arises from strain accumulation, bubble-induced fatigue, galvanic and potential-driven corrosion, selective leaching, and phase relaxation, with these pathways often proceeding simultaneously across multiple length scales. Such complexity helps explain why durability assessments based solely on conventional electrochemical metrics can be misleading. Emerging operando techniques provide a more accurate view of these transformations and highlight the importance of correlating electrochemical measurements with direct visualization of interfacial changes. These insights suggest that future efforts should consider mechanical, electrochemical, and electronic degradation processes when designing heterostructures, with this simultaneous addressing enabling the development of robust and stable 2D heterostructures for practical electrochemical energy conversion.

Author Contributions: O.P.G. performed the investigation and wrote the original draft. M.H. provided resources. M.H. and D.-R.C. reviewed and edited the manuscript and supervised the project. All authors have read and agreed to the published version of the manuscript.

Funding: This work was financially supported by the National Science and Technology Council (NSTC), Taiwan under grants 114-2112-M-033-013-MY3.

Data Availability Statement: This work is based on previously published materials, which have been duly referenced. No new data were created or analyzed in this study.

Conflicts of Interest: The authors declare no conflicts of interest.

References

1. Song, B.; Xia, X.; Ma, Z.; Li, R.; Wang, X.; Zhou, L.; Huang, Y. Breaking the Linear Scaling Relationship by Alloying Micro Sn to a Cu Surface toward CO_2 Electrochemical Reduction. *J. Phys. Chem. Lett.* **2024**, *15*, 9342–9348. [CrossRef]
2. He, J.; Liang, Y.; Mao, J.; Zhang, X.; Yang, X.; Cui, Z.; Zhu, S.; Li, Z.; Li, B. 3D Tungsten-doped MoS_2 nanostructure: A low-cost, facile prepared catalyst for hydrogen evolution reaction. *J. Electrochem. Soc.* **2016**, *163*, H299–H304. [CrossRef]
3. Zhang, X.; Chen, A.; Chen, L.; Zhou, Z. 2D materials bridging experiments and computations for electro/photocatalysis. *Adv. Energy Mater.* **2022**, *12*, 2003841. [CrossRef]
4. Cho, Y.S.; Kang, J. Two-dimensional materials as catalysts, interfaces, and electrodes for an efficient hydrogen evolution reaction. *Nanoscale* **2024**, *16*, 3936–3950. [CrossRef]

5. Shi, Z.; Yang, W.; Gu, Y.; Liao, T.; Sun, Z. Metal-nitrogen-doped carbon materials as highly efficient catalysts: Progress and rational design. *Adv. Sci.* **2020**, *7*, 2001069. [CrossRef]
6. Shifa, T.A.; Wang, F.; Liu, Y.; He, J. Heterostructures based on 2D materials: A versatile platform for efficient catalysis. *Adv. Mater.* **2019**, *31*, 1804828. [CrossRef]
7. Deng, D.; Novoselov, K.; Fu, Q.; Zheng, N.; Tian, Z.; Bao, X. Catalysis with two-dimensional materials and their heterostructures. *Nat. Nanotechnol.* **2016**, *11*, 218–230. [CrossRef]
8. Song, B.; Jin, S. Two are better than one: Heterostructures improve hydrogen evolution catalysis. *Joule* **2017**, *1*, 220–221. [CrossRef]
9. Li, J.; Yang, X.; Liu, Y.; Huang, B.; Wu, R.; Zhang, Z.; Zhao, B.; Ma, H.; Dang, W.; Wei, Z.; et al. General synthesis of two-dimensional van der Waals heterostructure arrays. *Nature* **2020**, *579*, 368–374. [CrossRef] [PubMed]
10. Zhang, C.; Luo, Y.; Tan, J.; Yu, Q.; Yang, F.; Zhang, Z.; Yang, L.; Cheng, H.-M.; Liu, B. High-throughput production of cheap mineral-based two-dimensional electrocatalysts for high-current-density hydrogen evolution. *Nat. Commun.* **2020**, *11*, 3724. [CrossRef] [PubMed]
11. Chen, D.-R.; Muthu, J.; Chang, J.-T.; Lin, P.-H.; Chen, Y.-X.; Khurshid, F.; Chin, H.-T.; Kong, J.; Hofmann, M.; Hsieh, Y.-P. Breaking Electrochemical Scaling Laws in Atomically Engineered van der Waals Stack Multisite Edge Catalysts. *Nano Lett.* **2025**, *25*, 12059–12066. [CrossRef] [PubMed]
12. Liu, J.; Zhang, S.; A, Y.; Li, Z.; Zhang, X.; Zhang, Y.; Guo, C.; Zhang, Z.; Du, M. Interfacial Electronic Engineering of the 2D/2D Cu-MoS_2/Cu_3(HIB)$_2$ Heterojunction for Bifunctional Ammonia Electrolysis: Synergistic Hydrogen Production and Wastewater Detoxification. *Adv. Funct. Mater.* **2025**, *36*, e14112. [CrossRef]
13. Hou, Z.; Cui, C.; Li, Y.; Gao, Y.; Zhu, D.; Gu, Y.; Pan, G.; Zhu, Y.; Zhang, T. Lattice-strain engineering for heterogenous electrocatalytic oxygen evolution reaction. *Adv. Mater.* **2023**, *35*, 2209876. [CrossRef] [PubMed]
14. Yuan, S.; Xia, M.; Liu, Z.; Wang, K.; Xiang, L.; Huang, G.; Zhang, J.; Li, N. Dual synergistic effects between Co and Mo_2C in Co/Mo_2C heterostructure for electrocatalytic overall water splitting. *Chem. Eng. J.* **2022**, *430*, 132697. [CrossRef]
15. Sekar, U.; Radhakrishnan, J.; Biswas, K. A review on the cooperative effect of intimate interfacial TMD/MXene (2D/2D) heterostructures for an enhanced electrocatalytic hydrogen evolution reaction. *Sustain. Energy Fuels* **2025**, *9*, 5399–5431. [CrossRef]
16. Wang, H.; Chen, D.-R.; Lin, Y.-C.; Lin, P.-H.; Chang, J.-T.; Muthu, J.; Hofmann, M.; Hsieh, Y.-P. Enhancing the electrochemical activity of 2D materials edges through oriented electric fields. *ACS Nano* **2024**, *18*, 19828–19835. [CrossRef]
17. Ding, T.; Jiang, X.; Quan, J.; Wang, R.; Li, M.; Lan, C.; Ma, W.; Zhu, M. Recent progress in two-dimensional van der Waals heterojunctions for flexible energy storage applications. *Adv. Compos. Hybrid Mater.* **2025**, *8*, 324. [CrossRef]
18. Sim, Y.; Kim, S.Y.; Park, S.D.; Lee, H.; Kim, J.; Jang, S.; Wang, J.; Song, S.; Kwak, J.; Lee, Z.; et al. Interfacial Control of Degradation Pathways in 2D Heterostructures. *Adv. Funct. Mater.* **2026**, *36*, e16434. [CrossRef]
19. Rokni, H.; Lu, W. Direct measurements of interfacial adhesion in 2D materials and van der Waals heterostructures in ambient air. *Nat. Commun.* **2020**, *11*, 5607. [CrossRef]
20. Zhu, H.; Liu, Y.; Wu, Y.; He, Y.; Cao, Y.; Hu, S. Electrocatalytic stability of two-dimensional materials. *J. Energy Chem.* **2024**, *97*, 302–320. [CrossRef]
21. Wang, L.; Chen, W.; Zhang, D.; Du, Y.; Amal, R.; Qiao, S.; Wu, J.; Yin, Z. Surface strategies for catalytic CO_2 reduction: From two-dimensional materials to nanoclusters to single atoms. *Chem. Soc. Rev.* **2019**, *48*, 5310–5349. [CrossRef] [PubMed]
22. Khan, K.; Tareen, A.K.; Aslam, M.; Zhang, Y.; Wang, R.; Ouyang, Z.; Gou, Z.; Zhang, H. Recent advances in two-dimensional materials and their nanocomposites in sustainable energy conversion applications. *Nanoscale* **2019**, *11*, 21622–21678. [CrossRef]
23. Wang, M.; Shi, H.; Tian, M.; Chen, R.; Shu, J.; Zhang, Q.; Wang, Y.; Li, C.; Wan, N.; Lei, S. Single nickel atom-modified phosphorene nanosheets for electrocatalytic CO_2 reduction. *ACS Appl. Nano Mater.* **2021**, *4*, 11017–11030. [CrossRef]
24. Liu, Y.; Wu, J.; Hackenberg, K.P.; Zhang, J.; Wang, Y.M.; Yang, Y.; Keyshar, K.; Gu, J.; Ogitsu, T.; Vajtai, R.; et al. Self-optimizing, highly surface-active layered metal dichalcogenide catalysts for hydrogen evolution. *Nat. Energy* **2017**, *2*, 17127. [CrossRef]
25. Yang, R.; Fan, Y.; Mei, L.; Shin, H.S.; Voiry, D.; Lu, Q.; Li, J.; Zeng, Z. Synthesis of atomically thin sheets by the intercalation-based exfoliation of layered materials. *Nat. Synth.* **2023**, *2*, 101–118. [CrossRef]
26. Zhou, Z.; Hou, F.; Huang, X.; Wang, G.; Fu, Z.; Liu, W.; Yuan, G.; Xi, X.; Xu, J.; Lin, J.; et al. Stack growth of wafer-scale van der Waals superconductor heterostructures. *Nature* **2023**, *621*, 499–505. [CrossRef]
27. Huang, G.; Chen, R.; Chen, M.; Chen, X.; Jiang, M.; Xing, Y.; Wang, J.; Liang, B.; Liu, Q.; Li, X.; et al. Transfer and beyond: Emerging strategies and trends in two-dimensional material device fabrication. *Chem. Soc. Rev.* **2026**, *55*, 2574–2634. [CrossRef]
28. Liu, Y.; Huang, Y.; Duan, X. Van der Waals integration before and beyond two-dimensional materials. *Nature* **2019**, *567*, 323–333. [CrossRef]
29. Miao, Y.; Zhao, Y.; Zhang, S.; Shi, R.; Zhang, T. Strain engineering: A boosting strategy for photocatalysis. *Adv. Mater.* **2022**, *34*, 2200868. [CrossRef] [PubMed]
30. Liu, G.; Wong, W.S.; Kraft, M.; Ager, J.W.; Vollmer, D.; Xu, R. Wetting-regulated gas-involving (photo) electrocatalysis: Biomimetics in energy conversion. *Chem. Soc. Rev.* **2021**, *50*, 10674–10699. [CrossRef]

31. Lu, Z.; Zhu, W.; Yu, X.; Zhang, H.; Li, Y.; Sun, X.; Wang, X.; Wang, H.; Wang, J.; Luo, J.; et al. Ultrahigh hydrogen evolution performance of under-water "superaerophobic" MoS_2 nanostructured electrodes. *Adv. Mater.* **2014**, *26*, 2683–2687. [CrossRef] [PubMed]
32. Iwata, R.; Zhang, L.; Wilke, K.L.; Gong, S.; He, M.; Gallant, B.M.; Wang, E.N. Bubble growth and departure modes on wettable/non-wettable porous foams in alkaline water splitting. *Joule* **2021**, *5*, 887–900. [CrossRef]
33. He, Y.; Liu, L.; Zhu, C.; Guo, S.; Golani, P.; Koo, B.; Tang, P.; Zhao, Z.; Xu, M.; Zhu, C.; et al. Amorphizing noble metal chalcogenide catalysts at the single-layer limit towards hydrogen production. *Nat. Catal.* **2022**, *5*, 212–221. [CrossRef]
34. Kalantar-Zadeh, K.; Ou, J.Z.; Daeneke, T.; Mitchell, A.; Sasaki, T.; Fuhrer, M.S. Two dimensional and layered transition metal oxides. *Appl. Mater. Today* **2016**, *5*, 73–89. [CrossRef]
35. Voiry, D.; Fullon, R.; Yang, J.; de Carvalho Castro e Silva, C.; Kappera, R.; Bozkurt, I.; Kaplan, D.; Lagos, M.J.; Batson, P.E.; Gupta, G.; et al. The role of electronic coupling between substrate and 2D MoS2 nanosheets in electrocatalytic production of hydrogen. *Nat. Mater.* **2016**, *15*, 1003–1009. [CrossRef]
36. Feng, Y.; Wang, C.; Ye, F.; Liu, H.; Yang, J. Effect of electronic coupling on the electrocatalytic performance of platinum metal. *RSC Adv.* **2016**, *6*, 80910–80915. [CrossRef]
37. Cai, M.; Wei, Y.; Li, Y.; Li, X.; Wang, S.; Shao, G.; Zhang, P. 2D semiconductor nanosheets for solar photocatalysis. *EcoEnergy* **2023**, *1*, 248–295. [CrossRef]
38. Nie, K.; Qu, X.; Gao, D.; Li, B.; Yuan, Y.; Liu, Q.; Li, X.; Chong, S.; Liu, Z. Engineering phase stability of semimetallic MoS_2 monolayers for sustainable electrocatalytic hydrogen production. *ACS Appl. Mater. Interfaces* **2022**, *14*, 19847–19856. [CrossRef]
39. Liu, H.; Xie, R.; Luo, Y.; Cui, Z.; Yu, Q.; Gao, Z.; Zhang, Z.; Yang, F.; Kang, X.; Ge, S.; et al. Dual interfacial engineering of a Chevrel phase electrode material for stable hydrogen evolution at 2500 mA cm^{-2}. *Nat. Commun.* **2022**, *13*, 6382. [CrossRef]
40. Sun, W.; Meng, A.; Wang, L.; Li, G.; Cui, J.; Sun, Y.; Li, Z. Defects and morphology engineering for constructing V_S-Ni_3S_2@V_S-Cu_2S nanotube heterojunction arrays toward efficient bifunctional electrocatalyst for overall water splitting. *J. Energy Chem.* **2024**, *94*, 29–40. [CrossRef]
41. Tsai, C.; Abild-Pedersen, F.; Nørskov, J.K. Tuning the MoS_2 edge-site activity for hydrogen evolution via support interactions. *Nano Lett.* **2014**, *14*, 1381–1387. [CrossRef] [PubMed]
42. Feng, Z.; Tang, Y.; Ma, Y.; Li, Y.; Dai, Y.; Ding, H.; Su, G.; Dai, X. Theoretical investigation of CO_2 electroreduction on N (B)-doped graphdiyne mononlayer supported single copper atom. *Appl. Surf. Sci.* **2021**, *538*, 148145. [CrossRef]
43. Wang, R.; Guo, Z.; Tan, X.; Zhang, J.; Yang, L.; Wang, W.; Cao, L.; Dong, B. Atmosphere plasma treatment and Co heteroatoms doping on basal plane of colloidal 2D VSe_2 nanosheets for enhanced hydrogen evolution. *Int. J. Hydrogen Energy* **2021**, *46*, 32425–32434. [CrossRef]
44. Wu, Y.; Sun, C.; Wang, H.; Ji, S.; Pollet, B.G.; Lu, J.; Tian, X.; Liang, H.; Wang, X.; Wang, R. Ni_2P nanoparticles-inserted NiFeP nanosheets with rich interfaces as efficient catalysts for the oxygen evolution reaction. *J. Alloys Compd.* **2022**, *903*, 163855. [CrossRef]
45. Zhang, R.; Huang, L.; Yu, Z.; Jiang, R.; Hou, Y.; Sun, L.; Zhang, B.; Huang, Y.; Ye, B.; Zhang, Y. Spherical cactus-like composite based on transition metals Ni, Co and Mn with 1D/2D bonding heterostructure for electrocatalytic overall water splitting. *Electrochim. Acta* **2019**, *323*, 134845. [CrossRef]
46. Kwon, I.S.; Kwak, I.H.; Kim, J.Y.; Abbas, H.G.; Debela, T.T.; Seo, J.; Cho, M.K.; Ahn, J.-P.; Park, J.; Kang, H.S. Two-dimensional MoS_2/Fe-phthalocyanine hybrid nanostructures as excellent electrocatalysts for hydrogen evolution and oxygen reduction reactions. *Nanoscale* **2019**, *11*, 14266–14275. [CrossRef]
47. Chen, J.; Li, F.; Tang, Y.; Tang, Q. Tuning the phase stability and surface HER activity of 1T′-MoS_2 by covalent chemical functionalization. *J. Mater. Chem. C* **2020**, *8*, 15852–15859. [CrossRef]
48. Jiménez-Morales, I.; Reyes-Carmona, A.; Dupont, M.; Cavaliere, S.; Rodlert, M.; Mornaghini, F.; Larsen, M.J.; Odgaard, M.; Zajac, J.; Jones, D.J.; et al. Correlation between the surface characteristics of carbon supports and their electrochemical stability and performance in fuel cell cathodes. *Carbon Energy* **2021**, *3*, 654–665. [CrossRef]
49. Sassenburg, M.; Kelly, M.; Subramanian, S.; Smith, W.A.; Burdyny, T. Zero-gap electrochemical CO_2 reduction cells: Challenges and operational strategies for prevention of salt precipitation. *ACS Energy Lett.* **2022**, *8*, 321–331. [CrossRef]
50. Hadrian, H.; Lee, C.W. Electrochemical CO_2 conversion in acidic media: A comprehensive review of catalysts and electrolytes. *Chem. Eng. J.* **2025**, *526*, 170891. [CrossRef]
51. Hao, Y.; Hu, F.; Zhu, S.; Sun, Y.; Wang, H.; Wang, L.; Wang, Y.; Xue, J.; Liao, Y.F.; Shao, M.; et al. MXene-regulated metal-oxide interfaces with modified intermediate configurations realizing nearly 100% CO_2 electrocatalytic conversion. *Angew. Chem. Int. Ed.* **2023**, *62*, e202304179. [CrossRef]
52. Zeng, J.; Castellino, M.; Bejtka, K.; Sacco, A.; Di Martino, G.; Farkhondehfal, M.A.; Chiodoni, A.; Hernández, S.; Pirri, C.F. Facile synthesis of cubic cuprous oxide for electrochemical reduction of carbon dioxide. *J. Mater. Sci.* **2021**, *56*, 1255–1271. [CrossRef]
53. Khezri, B.; Fisher, A.C.; Pumera, M. CO_2 reduction: The quest for electrocatalytic materials. *J. Mater. Chem. A* **2017**, *5*, 8230–8246. [CrossRef]

54. Rabiee, H.; Ge, L.; Zhao, J.; Zhang, X.; Li, M.; Hu, S.; Smart, S.; Rufford, T.E.; Zhu, Z.; Wang, H.; et al. Regulating the reaction zone of electrochemical CO_2 reduction on gas-diffusion electrodes by distinctive hydrophilic-hydrophobic catalyst layers. *Appl. Catal. B Environ.* **2022**, *310*, 121362. [CrossRef]
55. Tan, Y.; Liu, P.; Chen, L.; Cong, W.; Ito, Y.; Han, J.; Guo, X.; Tang, Z.; Fujita, T.; Hirata, A.; et al. Monolayer MoS_2 films supported by 3D nanoporous metals for high-efficiency electrocatalytic hydrogen production. *Adv. Mater.* **2014**, *26*, 8023–8028. [CrossRef] [PubMed]
56. Lee, S.; Su, L.; Mesnier, A.; Cui, Z.; Manthiram, A. Cracking vs. surface reactivity in high-nickel cathodes for lithium-ion batteries. *Joule* **2023**, *7*, 2430–2444. [CrossRef]
57. Zhao, L.; Wen, M.; Tian, Y.; Wu, Q.; Fu, Y. A novel structure of quasi-monolayered NiCo-bimetal-phosphide for superior electrochemical performance. *J. Energy Chem.* **2022**, *74*, 203–211. [CrossRef]
58. Peng, W.; Luo, M.; Xu, X.; Jiang, K.; Peng, M.; Chen, D.; Chan, T.S.; Tan, Y. Spontaneous atomic ruthenium doping in Mo_2CT_X MXene defects enhances electrocatalytic activity for the nitrogen reduction reaction. *Adv. Energy Mater.* **2020**, *10*, 2001364. [CrossRef]
59. Chen, X.; Zhang, S.; Qian, X.; Liang, Z.; Xue, Y.; Zhang, X.; Tian, J.; Han, Y.; Shao, M. Enabling efficient electrocatalytic conversion of N_2 to NH_3 by Ti_3C_2 MXene loaded with semi-metallic 1T′-MoS_2 nanosheets. *Appl. Catal. B Environ.* **2022**, *310*, 121277. [CrossRef]
60. King, L.A.; Hubert, M.A.; Capuano, C.; Manco, J.; Danilovic, N.; Valle, E.; Hellstern, T.R.; Ayers, K.; Jaramillo, T.F. A non-precious metal hydrogen catalyst in a commercial polymer electrolyte membrane electrolyser. *Nat. Nanotechnol.* **2019**, *14*, 1071–1074. [CrossRef]
61. Xu, Y.; Ge, R.; Yang, J.; Li, J.; Li, S.; Li, Y.; Zhang, J.; Feng, J.; Liu, B.; Li, W. Molybdenum disulfide (MoS_2)-based electrocatalysts for hydrogen evolution reaction: From mechanism to manipulation. *J. Energy Chem.* **2022**, *74*, 45–71. [CrossRef]
62. Wang, S.; Lu, A.; Zhong, C.-J. Hydrogen production from water electrolysis: Role of catalysts. *Nano Converg.* **2021**, *8*, 4. [CrossRef]
63. Chen, R.; Hung, S.F.; Zhou, D.; Gao, J.; Yang, C.; Tao, H.; Yang, H.B.; Zhang, L.; Zhang, L.; Xiong, Q.; et al. Layered structure causes bulk NiFe layered double hydroxide unstable in alkaline oxygen evolution reaction. *Adv. Mater.* **2019**, *31*, 1903909. [CrossRef] [PubMed]
64. Islam, M.S.; Kim, M.; Jin, X.; Oh, S.M.; Lee, N.-S.; Kim, H.; Hwang, S.-J. Bifunctional 2D superlattice electrocatalysts of layered double hydroxide–transition metal dichalcogenide active for overall water splitting. *ACS Energy Lett.* **2018**, *3*, 952–960. [CrossRef]
65. Escalera-López, D.; Iffelsberger, C.; Zlatar, M.; Novčić, K.; Maselj, N.; Van Pham, C.; Jovanovič, P.; Hodnik, N.; Thiele, S.; Pumera, M.; et al. Allotrope-dependent activity-stability relationships of molybdenum sulfide hydrogen evolution electrocatalysts. *Nat. Commun.* **2024**, *15*, 3601. [CrossRef]
66. Shen, T.-H.; Spillane, L.; Peng, J.; Shao-Horn, Y.; Tileli, V. Switchable wetting of oxygen-evolving oxide catalysts. *Nat. Catal.* **2022**, *5*, 30–36. [CrossRef] [PubMed]
67. Lu, Y.; Li, B.; Xu, N.; Zhou, Z.; Xiao, Y.; Jiang, Y.; Li, T.; Hu, S.; Gong, Y.; Cao, Y. One-atom-thick hexagonal boron nitride co-catalyst for enhanced oxygen evolution reactions. *Nat. Commun.* **2023**, *14*, 6965. [CrossRef]
68. Huang, T.-X.; Cong, X.; Wu, S.-S.; Wu, J.-B.; Bao, Y.-F.; Cao, M.-F.; Wu, L.; Lin, M.-L.; Wang, X.; Tan, P.-H.; et al. Visualizing the structural evolution of individual active sites in MoS2 during electrocatalytic hydrogen evolution reaction. *Nat. Catal.* **2024**, *7*, 646–654. [CrossRef]
69. Deng, J.; Ren, P.; Deng, D.; Bao, X. Enhanced electron penetration through an ultrathin graphene layer for highly efficient catalysis of the hydrogen evolution reaction. *Angew. Chem. Int. Ed.* **2015**, *54*, 2100–2104. [CrossRef]
70. Liu, M.; Wang, J.-A.; Klysubun, W.; Wang, G.-G.; Sattayaporn, S.; Li, F.; Cai, Y.-W.; Zhang, F.; Yu, J.; Yang, Y. Interfacial electronic structure engineering on molybdenum sulfide for robust dual-pH hydrogen evolution. *Nat. Commun.* **2021**, *12*, 5260. [CrossRef]
71. Song, J.; Wei, C.; Huang, Z.-F.; Liu, C.; Zeng, L.; Wang, X.; Xu, Z.J. A review on fundamentals for designing oxygen evolution electrocatalysts. *Chem. Soc. Rev.* **2020**, *49*, 2196–2214. [CrossRef]
72. Du, Y.; Li, B.; Xu, G.; Wang, L. Recent advances in interface engineering strategy for highly-efficient electrocatalytic water splitting. *InfoMat* **2023**, *5*, e12377. [CrossRef]
73. Jia, Y.; Zhang, L.; Gao, G.; Chen, H.; Wang, B.; Zhou, J.; Soo, M.T.; Hong, M.; Yan, X.; Qian, G.; et al. A heterostructure coupling of exfoliated Ni–Fe hydroxide nanosheet and defective graphene as a bifunctional electrocatalyst for overall water splitting. *Adv. Mater.* **2017**, *29*, 1700017. [CrossRef]
74. Yang, F.; Hu, P.; Yang, F.F.; Chen, B.; Yin, F.; Hao, K.; Sun, R.; Gao, L.; Sun, Z.; Wang, K.; et al. CNTs bridged basal-plane-active 2H-MoS_2 nanosheets for efficient robust electrocatalysis. *Small* **2023**, *19*, 2301468. [CrossRef]
75. Yu, L.; Deng, D.; Bao, X. Chain mail for catalysts. *Angew. Chem. Int. Ed.* **2020**, *59*, 15294–15297. [CrossRef] [PubMed]
76. Fang, W.; Huang, L.; Zaman, S.; Wang, Z.; Han, Y.; Xia, B.Y. Recent progress on two-dimensional electrocatalysis. *Chem. Res. Chin. Univ.* **2020**, *36*, 611–621. [CrossRef]

77. Zhang, H.; Li, X.; Hähnel, A.; Naumann, V.; Lin, C.; Azimi, S.; Schweizer, S.L.; Maijenburg, A.W.; Wehrspohn, R.B. Bifunctional heterostructure assembly of NiFe LDH nanosheets on NiCoP nanowires for highly efficient and stable overall water splitting. *Adv. Funct. Mater.* **2018**, *28*, 1706847. [CrossRef]
78. Suryawanshi, U.P.; Ghorpade, U.V.; Lee, D.M.; He, M.; Shin, S.W.; Kumar, P.V.; Jang, J.S.; Jung, H.R.; Suryawanshi, M.P.; Kim, J.H. Colloidal Ni_2P nanocrystals encapsulated in heteroatom-doped graphene nanosheets: A synergy of 0D@2D heterostructure toward overall water splitting. *Chem. Mater.* **2020**, *33*, 234–245. [CrossRef]
79. Liu, X.; Guo, R.; Ni, K.; Xia, F.; Niu, C.; Wen, B.; Meng, J.; Wu, P.; Wu, J.; Wu, X.; et al. Reconstruction-determined alkaline water electrolysis at industrial temperatures. *Adv. Mater.* **2020**, *32*, 2001136. [CrossRef]
80. Cui, C.; Cheng, R.; Zhang, H.; Zhang, C.; Ma, Y.; Shi, C.; Fan, B.; Wang, H.; Wang, X. Ultrastable MXene@Pt/SWCNTs′ nanocatalysts for hydrogen evolution reaction. *Adv. Funct. Mater.* **2020**, *30*, 2000693. [CrossRef]
81. Ye, Q.; Man, J.; Huang, Y.; Hao, W.; Zhao, P.; Dou, M.; Wang, F. Carbon-Bifunctionalized Mo_2N Coupled Atomic Pb Sites for Efficient Nitrogen Reduction. *Small* **2026**, *22*, e11794. [CrossRef] [PubMed]

Disclaimer/Publisher's Note: The statements, opinions and data contained in all publications are solely those of the individual author(s) and contributor(s) and not of MDPI and/or the editor(s). MDPI and/or the editor(s) disclaim responsibility for any injury to people or property resulting from any ideas, methods, instructions or products referred to in the content.